

Pygmy and Giant Dipole Resonances by Coulomb Excitation using a Quantum Molecular Dynamics model

C. Tao,^{1,2} Y. G. Ma,^{1,*} G. Q. Zhang,¹ X. G. Cao,¹ D. Q. Fang,¹ and H. W. Wang¹

¹*Shanghai Institute of Applied Physics, Chinese Academy of Sciences, Shanghai 201800, China*

²*University of the Chinese Academy of Sciences, Beijing 100080, China*

(Dated: October 29, 2018)

Pygmy and Giant Dipole Resonance (PDR and GDR) in Ni isotopes have been investigated by Coulomb excitation in the framework of the Isospin-dependent Quantum Molecular Dynamics model (IQMD). The spectra of γ rays are calculated and the peak energy, the strength and Full Width at Half Maximum (FWHM) of GDR and PDR have been extracted. Their sensitivities to nuclear equation of state, especially to its symmetry energy term are also explored. By a comparison with the other mean-field calculations, we obtain the reasonable values for symmetry energy and its slope parameter at saturation, which gives an important constrain for IQMD model. In addition, we also studied the neutron excess dependence of GDR and PDR parameters for Ni isotopes and found that the energy-weighted sum rule (EWSR) $PDR_{m_1}/GDR_{m_1}\%$ increases linearly with the neutron excess.

PACS numbers: 25.75.Dw, 25.70.De, 25.70.Ef

I. INTRODUCTION

Intermediate energy heavy-ion collisions provide a chance to study reaction mechanism and the properties of hot nuclei, such as fragmentation and liquid gas phase transition etc [1–5]. In a relative low excitation region of nuclei, dipole resonance has attracted much attention experimentally and theoretically in the past few decades [6, 7]. Two kind of resonances have been evidenced, one is Pygmy Dipole Resonance (PDR) and another is Giant Dipole Resonance (GDR). In contrast to GDR, which can be considered as the oscillation between non-deformed, incompressible proton and neutron spheres, PDR can be considered as the oscillation between the weakly-bound neutron skin and the isospin neutral proton-neutron core. From a theoretical point of view, the presence of this low-lying strength PDR is predicted by almost all microscopic models, ranging from Hartree-Fock plus random phase approximation (RPA) with Skyrme interactions to relativistic Hartree-Bogoliubov plus relativistic quasiparticle RPA [7]. Experiments of PDR [8–14] in neutron-rich nuclei and microscopic models which have been applied to investigate PDR [15–21] have shown that the PDR could have a pronounced relationship with neutron-capture rates in the γ -process, nucleosynthesis, the radiative neutron-capture cross section on neutron-rich nuclei, and the photodisintegration of ultra-high energy cosmic rays. The properties of the PDR in stable nuclei have been studied extensively for different neutron and proton shell closures with the (γ, γ') reactions. However, studies for neutron-rich isotopes, where the PDR should be enhanced, were still less, especially in the framework of molecular-dynamics type model. Recently, the influ-

ence of symmetry energy on PDR has been also checked [22?]. For example, in Ref. [?], they studied isovector giant and pygmy dipole resonances in even-even Ni isotopes within the framework of a fully consistent relativistic random-phase approximation built on the relativistic mean field ground state and found that the centroid energy of the isovector pygmy resonance is insensitive to the density dependence of the symmetry energy. Ref.[22] used a semiclassical Landau-Vlasov approach to investigate the energy centroid associated with the PDR and found that PDR is insensitive to the symmetry energy term of EOS. Considering symmetry energy is one of interesting topics in current heavy-ion physics community, we would also like to check this sensitivity in the present work.

In this work, we apply the Isospin-dependent Quantum Molecular Dynamics model (IQMD) to investigate the properties of PDR. In our previous work, the same model has been successfully applied into the GDR calculation. Here we plan to extend the model to calculate PDR in the same framework. The molecular dynamics model is a kind of Monte-Carlo transport model, which has been extensively applied in heavy-ion collision dynamics. In the model, the physical parameters can be controlled and then their respective effects on PDR and GDR can be addressed.

The paper is organized as follows. Sec. II gives a brief introduction of IQMD model as well as the formalism to calculation GDR and PDR in the IQMD framework. Results and discussions are presented in Sec. III where different parameter dependencies of GDR and PDR are shown. In particular, the equation of state, symmetry energy and isospin effects are presented and discussed. Finally the summary is given in Sec. IV.

*Author to whom all correspondence should be addressed. Email: ygma@sinap.ac.cn

II. MODEL AND FORMALISM

The isospin-dependent quantum molecular dynamics (IQMD) model is based on QMD model [23]. In IQMD model, the mean field is given by: $U(\rho) = U^{Sky} + U^{Coul} + U^{Yuk} + U^{sym} + U^{MDI}$, where U^{Sky} , U^{Coul} , U^{Yuk} , U^{sym} and U^{MDI} is the Skyrme potential, Coulomb potential, Yukawa potential, symmetry potential interaction, and the momentum dependent interaction (MDI), respectively. The Skyrme potential can be presented as follows:

$$U^{Sky} = \alpha(\rho/\rho_0) + \beta(\rho/\rho_0)^\gamma, \quad (1)$$

where $\rho_0 = 0.16/fm^3$ (the saturation nuclear density) and ρ is the nuclear density. In the equation, different $[\alpha, \beta, \gamma]$ represents different kinds of equations of state (EOS). The parameters α , β and γ are given in Table I. In the Table, S(M) represents the soft EOS (with MDI), with an incompressibility of $K=200$ MeV, while H(M) for the hard EOS(with MDI), with an incompressibility of $K=380$ MeV.

TABLE I: The parameters α , β and γ for the different EOS

EOS	K (MeV)	α (MeV)	β (MeV)	γ (MeV)
S	200	-356	303	7/6
SM	200	-390.1	320.3	1.14
H	380	-124	70.5	2
HM	380	-129.2	59.4	2.09

U^{Coul} , U^{Yuk} , U^{sym} and U^{MDI} can be expressed as follows, respectively:

$$U^{Coul} = \frac{e^2}{4} \sum_{i \neq j} \frac{1}{(4\pi L)^{(3/2)}} \exp[-\frac{|r_i - r_j|^2}{4L}]. \quad (2)$$

Here, $r_{ij} = |\mathbf{r}_i - \mathbf{r}_j|$ represents the relative distance of two nucleons, and the L is the so-called Gaussian wave-packet width for nucleons. For simplicity, here we choose a constant wave-packet width, i.e. $L = 2.16 fm^2$. We noted that there was some discussions on the affect of the width on the dynamical results, eg. flow, multifragmentation, pion and kaon production etc [24]. However, we are treating the Coulomb excitation of the projectile in which the dynamical effect is relatively smaller.

$$U^{Yuk} = (V_y/2) \sum_{i \neq j} \frac{1}{\tau_{ij}} \exp(Lm^2) \times [\exp(mr_{ij}) \operatorname{erfc}(\sqrt{L}m - r_{ij}/\sqrt{4L}) - \exp(mr_{ij}) \operatorname{erfc}(\sqrt{L}m + r_{ij}/\sqrt{4L})], \quad (3)$$

where $V_y=0.0024$ GeV and $m = 0.83$.

$$U^{sym} = \frac{C_{sym}}{2\rho_0} \sum_{i \neq j} \tau_{iz} \tau_{jz} \frac{1}{(4\pi L)^{3/2}} \exp[-\frac{(\mathbf{r}_i - \mathbf{r}_j)^2}{4L}], \quad (4)$$

where C_{sym} is the symmetry energy coefficient, τ_z is the z th component of the isospin degree of freedom for the

nucleon, which equals 1 or -1 for neutron or proton, respectively.

$$U^{MDI} = \delta \ln^2[\varepsilon(\frac{\rho}{\rho_0})^2 + 1](\frac{\rho}{\rho_0}), \quad (5)$$

Here, $\delta = 1.57$ MeV and $\varepsilon = 500 c^2/GeV^2$. More details of the QMD model can be found in [23, 25–28].

The dipole moment of GDR in coordinator space [$DR_{GDR}(t)$] and momentum space [$DK_{GDR}(t)$] is respectively defined as follows [29, 30]:

$$DR_{GDR}(t) = \frac{NZ}{A} [R_Z(t) - R_N(t)], \quad (6)$$

$$DK_{GDR}(t) = \frac{NZ}{A\hbar} [\frac{P_Z(t)}{Z} - \frac{P_N(t)}{N}], \quad (7)$$

where $R_Z(t)$ and $R_N(t)$ are the center of mass of protons and neutrons in coordinator space, respectively; $P_Z(t)$ and $P_N(t)$ are the center of mass of protons and neutrons in momentum space, respectively.

By the Fourier transformation of the second derivative of $DR_{GDR}(t)$ in respect to time, i.e.

$$DR''(\omega) = \int_{t_0}^{t_{max}} DR''(t) e^{i\omega t} dt, \quad (8)$$

we can get the the γ ray emission probability for energy $E_\gamma = \hbar\omega$ as follow:

$$\frac{dP}{dE_\gamma} = \frac{2e^2}{3\pi\hbar c^3 E_\gamma} |DR''(\omega)|^2. \quad (9)$$

Similarly, we can write the dipole moment of PDR in coordinator space and momentum space as follows:

$$DR_{PDR}(t) = \frac{N_v Z}{A} [R_C(t) - R_{N_v}(t)], \quad (10)$$

$$DK_{PDR}(t) = \frac{N_v Z}{A\hbar} [\frac{P_C(t)}{2Z} - \frac{P_{N_v}(t)}{N_v}], \quad (11)$$

where $R_C(t)$ and $R_{N_v}(t)$ are the center of mass of isospin-symmetric core and valence neutrons in coordinator space, respectively; $P_Z(t)$ and $P_N(t)$ are the center of mass of isospin-symmetric core and valence neutrons in momentum space, respectively. Then we can also get the γ ray emission probability of PDR. Here, we choose neutrons with the farthest distances from the CM of all nucleons as the valence neutrons in the initial state.

The fraction of the energy-weighted sum rule (EWSR) contained in the PDR relative to that located in the GDR region can be written as follows

$$m_1\% = \frac{PDR_{m_1}}{GDR_{m_1}} \times 100\%, \quad (12)$$

where GDR_{m_1} and PDR_{m_1} is EWSR of GDR and PDR,

respectively:

$$GDR_{m_1} = \sum_{E_1}^{E_2} \left(\frac{dP}{dE_\gamma} \right)_{GDR} \Delta E \times E, \quad (13)$$

$$PDR_{m_1} = \sum_{E'_1}^{E'_2} \left(\frac{dP}{dE_\gamma} \right)_{PDR} \Delta E \times E. \quad (14)$$

III. RESULTS AND DISCUSSIONS

Now we move on the calculations and discussions. As a first step of this work, we need to check the stability of the nuclei [27]. Here we select $^{68}\text{Ni}+^{197}\text{Au}$ as an example, where the Soft EOS with MDI has been used. Figure 1 displays the binding energies and root mean square radii of the cold projectile (^{68}Ni) and target (^{197}Au) nuclei as a function of time till 400 fm/c. It is clearly seen that both variables keep very stable during the whole time evolution, which assures that we can proceed with the following calculations on the GDR and PDR.

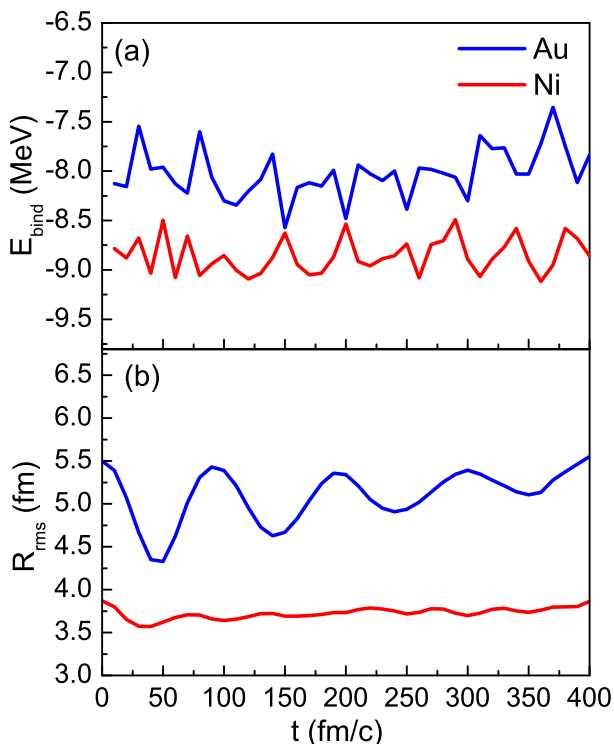


FIG. 1: (Color online) Stability check for the projectile (^{68}Ni) and target (^{197}Au). (a) time evolution of the binding energies; (b) time evolution of rms radii.

After the stability check, we shall compare the calculated results with the experimental data to demonstrate the reliability of our calculation. The calculation parameters are as follows: incident energy (E_{in}) is 600

MeV/nucleon, impact parameter (b) is 24fm, the Soft EOS with MDI, and C_{sym} is 32MeV. The PDR result of ^{68}Ni is shown in Figure 2 where the symbol with error bar is for the experimental data from Ref. [11], the line is our calculated result. We can see that the peak energy of our calculated result has good agreement with the data even though the FWHM of our calculated result is a little larger than the data. For GDR calculations, our previous IQMD calculations have shown a good agreement with the data [30]. After this comparison, we perform a systematic calculation to explore the variable dependencies of GDR and PDR.

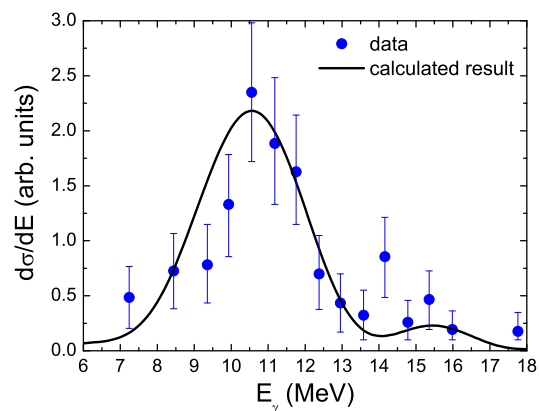


FIG. 2: (Color online) The calculated PDR result of ^{68}Ni compared with the experimental data. The blue circle with error bar is the experimental data in Ref. [11], the black line is the calculated result.

Firstly, the sensitivities of GDR and PDR of ^{68}Ni in the Coulomb excitation of ^{197}Au to some parameters have been studied. From the calculated results, we can extract the peak energy, strength and FWHM of GDR or PDR by Gaussian fitting to the γ emission spectrum. Figure 3 shows the time evolution of dipole moment for GDR and PDR at different incident energies. With an increasing of energy, both amplitude and frequency of GDR and PDR oscillations become smaller, this could be attributable to the weakening of the effective Coulomb field in which the projectile interacts with the target when the projectile has faster velocity. Actually this can be seen from the inverse of the distance ($1/R_{PT}$) between the CM of protons of projectile and CM of protons of target. Figure 4 shows $1/R_{PT}$ as a function of time in different incident energies. If we roughly treat the projectile and target as point charged particles, then the Coulomb interaction is proportional to the time integration of $1/R_{PT}$. Therefore, the Coulomb effect becomes smaller when the incident energy is larger and then the projectile gets less excited.

On the other hand, in Figure 3 pygmy dipole oscillation shows a much smaller amplitude and a slightly smaller frequency in comparison with the GDR case. These lead to the behavior of the incident energy dependence of the

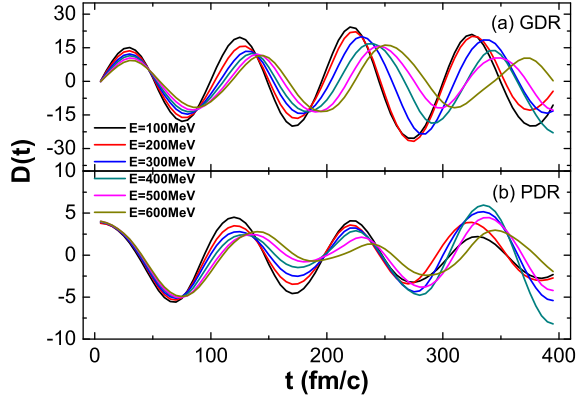


FIG. 3: (Color online) Time evolution of dipole moment for GDR (a) and PDR (b) at different incident energies. The meaning of lines are illustrated in the insert. In calculations, we use $b = 24$ fm, $C_{sym} = 32$ MeV, and the Soft EOS without MDI.

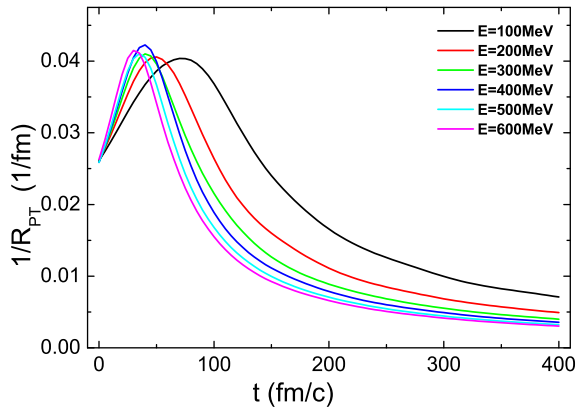


FIG. 4: (Color online) Time evolution of dipole moment for GDR and PDR at different incident energies. The meaning of lines are illustrated in the insert. In calculations, we use $b = 24$ fm, $C_{sym} = 32$ MeV, and the Soft EOS without MDI.

GDR and PDR parameters as shown in Figure 5. With the increase of incident energy, both the peak energies and strength for GDR and PDR drop. For the FWHM, it clearly shows an increasing behavior for GDR. Similarly, FWHM of PDR displays an increasing behavior versus energy within large errors.

Figure 6 shows EOS dependence of the dipole resonance parameters. Compared to the Soft EOS with or without momentum dependent interaction, the calculated results with the Hard EOS are generally bigger. On the other hand, compared to the EOS without MDI, all the peak energy, strength and FWHM in the EOS with MDI are also larger. In this sense, MDI has similar effect to make the EOS harder. From this figure, we learn that dipole γ -emission is very sensitive to the stiffness of EOS.

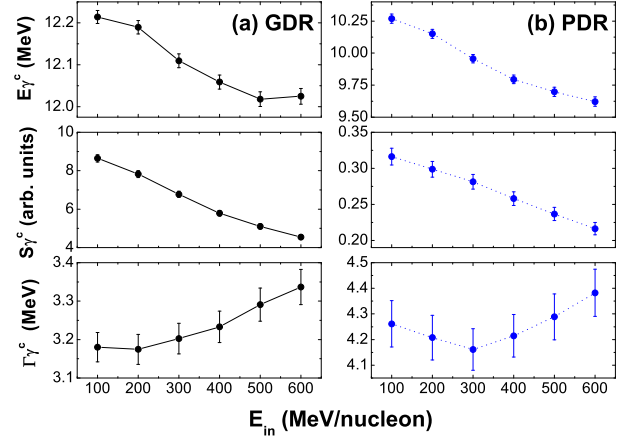


FIG. 5: (Color online) Incident energy dependence of dipole moments for ^{68}Ni . The upper panel for GDR and the bottom one for PDR. In calculations, we use $b = 24$ fm, $C_{sym} = 32$ MeV, and the Soft EOS without MDI.

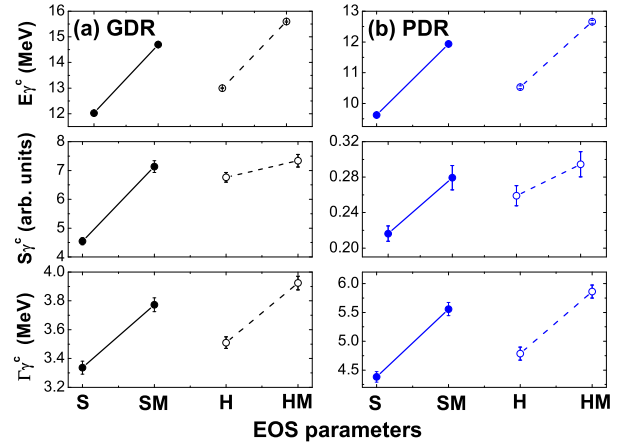


FIG. 6: (Color online) EOS dependencies of GDR (left panels) and PDR (right panels) parameters for ^{68}Ni . In calculations, we use $E_{in} = 600$ MeV/nucleon, $b = 24$ fm, and $C_{sym} = 32$ MeV.

Many works have demonstrated that the symmetry energy plays an important role in understanding the mechanisms of many exotic phenomena in nuclear physics and astrophysics. Dipole oscillations between all neutrons and all protons or between the excess neutrons and a core composed of an equal number of protons and neutrons involve asymmetry of neutron and proton, which could be influenced by the symmetry energy term of the EOS. To this end, we change the value of C_{sym} in IQMD model to address its effect on GDR and PDR. In order to see a clear trend of GDR and PDR toward the symmetry energy coefficient, we choose a larger range of C_{sym} in the calculations, i.e. from 16 - 64 MeV. In between, a value of C_{sym} around 36 MeV has been thought reason-

able to describe the property of ground state of nuclei in many previous studies. Figure 7 shows time evolution of dipole moments for GDR (upper panel) and PDR (lower panel) in different symmetry coefficients C_{sym} . It shows that the frequency of GDR oscillations becomes faster and the amplitude tends to be smaller with the increasing of C_{sym} , which leads to an increasing of peak energy and decreasing of strength as shown in next figure. On the contrary, the frequency of PDR oscillations becomes slightly slower, but the amplitude tends to be smaller as well as GDR with the increasing of C_{sym} , which induces a decreasing of peak energy as well as strength as shown in next figure.

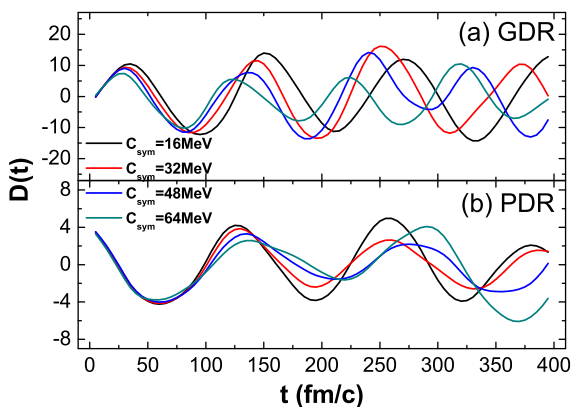


FIG. 7: (Color online) C_{sym} dependence of dipole moments for ^{68}Ni . The upper panel for GDR and the bottom one for PDR. In calculations, we use $E_{in} = 600$ MeV/nucleon, $b = 24$ fm, and the Soft EOS without MDI.

Figure 8 shows the calculated results of PDR and GDR parameters with the different C_{sym} parameters. With the increases of C_{sym} , the peak energies of GDR show a linear increase, but those of PDR shows a little decrease. However, considering the obvious different scale in y-axis for GDR and PDR, peak energy of PDR has only about 4% decrease in contrast to 25% increase for GDR. For strength, both show a decreasing behavior and for FWHM, both display an increasing trend. In some previous studies, it was known that the restoring force of isovector GDR is proportional to the symmetry energy of nuclear matter, which makes the peak energies of GDR pushed to higher energies with stronger symmetry energy. By contrast, PDR originates mainly from the vibrations of a few valence neutrons which against the isospin neutral core. Those valence neutrons are located in the very low density exterior region, where the symmetry energy is not affected as much. In general, the main difference by C_{sym} is observed in the interior region where is responsible for GDR, which has very little or weak influence on the subtle properties of PDR. Similar insensitivity of PDR to symmetry energy was also found in some literatures [22?].

It will be very interesting if we can pin down some in-

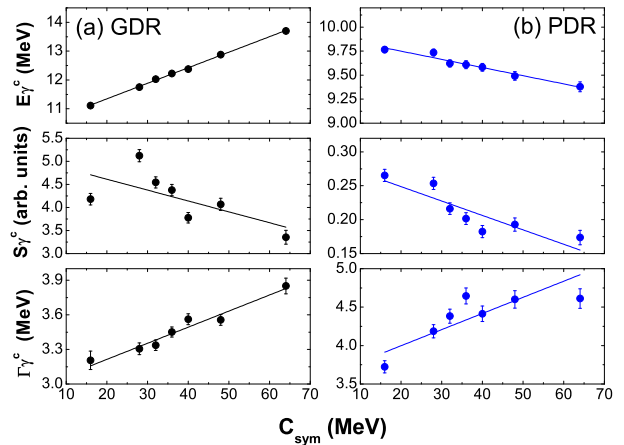


FIG. 8: (Color online) C_{sym} dependence of GDR (left panels) and PDR (right panels) parameters for ^{68}Ni . Symbols present for calculations and curves are linear fits for guiding the eyes. In calculations, we use $E_{in} = 600$ MeV/nucleon, $b = 24$ fm, and the Soft EOS without MDI.

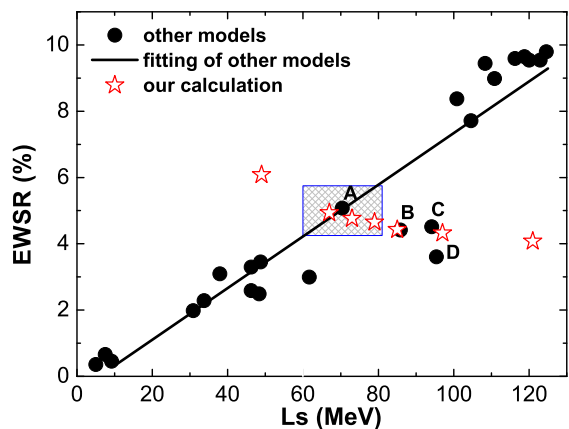


FIG. 9: (Color online) Calculated EWSR ($PDR_{m_1}/(PDR_{m_1} + GDR_{m_1})\%$) for ^{68}Ni with different E_{sym} in our IQMD model (open stars) together with a bunch of mean-field model calculations (solid circles), which is taken from Ref. [31]. Line is a fit to mean-field model calculations. In the figure, A, B, C and D represent mean-field calculations with SkMP, SkRs, SkGs, and SK255 parametrization. For details, see Ref. [31]. In figure, the shaded area represents 15% uncertainty around the point A which is just on fitted line.

formation on the symmetry energy, such as the $E_{sym}(\rho_0)$ and the derivative of the symmetry energy at saturation (L_s) by the dipole resonance calculation. In our IQMD model, the symmetry energy reads

$$E_{sym} = 12.5\left(\frac{\rho}{\rho_0}\right)^{2/3} + \frac{C_{sym}}{2}\left(\frac{\rho}{\rho_0}\right), \quad (15)$$

where the first term is the kinetic energy contribution and the second term is potential energy term. In this case, the slope parameter of the symmetry energy at saturation, $L_s = 3C_{sym}/2 + 25$. With the various C_{sym} , we can obtain a plot of EWSR $PDR_{m_1}/(PDR_{m_1} + GDR_{m_1})\%$ versus L_s as shown in Figure 9. To compare with other model calculations, different mean-field calculation results [31] for ^{68}Ni are displayed in the figure. From the figure, we observe a weak anticorrelation of EWSR vs L_s in IQMD calculations. However, the IQMD results are quite similar to the mean-field calculations with SkMP, SkRs, SkGs, and SK255 parameterizations, i.e. the corresponding A, B, C and D points [31]. The anticorrelation is not so reasonable in comparison with the overall positive correlation trend which has been constructed by the mean-field calculations from $L_s \approx 10$ -120 MeV. This may originate from the unreal symmetry energy coefficient when C_{sym} is selected too large or too smaller. Assuming the fitting line is correct for the relationship of EWSR versus L_s and allow 15% uncertainty, we can obtain that the reasonable L_s values from 60 to 81 MeV for IQMD calculations (see the shaded area), which leads to $C_{sym} \approx 23.3 - 37.3$ MeV, and gives $E_{sym}(\rho_0) \approx 24.2 - 31.2$ MeV. The above values for IQMD are in good agreement with other calculations. For instance, in Ref. [31], they got the weighted average, $L_s = 64.8 \pm 15.7$ MeV, and the deduced best value of $E_{sym}(\rho_0) = 32.3 \pm 1.3$ MeV. In Ref. [32] they give the value of $E_{sym}(\rho_0) = 32.0 \pm 1.8$ MeV and in Ref. [33] the ranges obtained of $E_{sym}(\rho_0)$ is 30.2 - 33.8 MeV. So far, the above $E_{sym}(\rho_0)$ and L parameters give a useful constraint for the IQMD model.

We also studied the systematic evolution of GDR and PDR parameters of even-even Ni isotopes from ^{62}Ni to ^{78}Ni . Figure 10 shows the distributions of isovector dipole strength for the Ni isotopes. In the figure, the GDR peak is around 12 MeV and that of PDR is around 10 MeV. The PDR strengths increase as the neutron number increases.

Figure 11 shows the extracted GDR and PDR parameters for Ni isotopes from Figure 10. With the increases of mass number A or neutron excess, the peak energies of both GDR and PDR decrease. This behavior reflects that a larger neutron excess results in lower GDR and PDR excitation energy. In the region beyond $A = 72$, the slope of the PDR peak energies becomes steeper than those of lower mass nuclei, because the neutrons in outer orbital are more loosely bound and thus the restoring force in the oscillation of the skin against the core becomes weaker. The strength of GDR is shown to seemingly decrease decreasing for larger mass nuclei but it increases for PDR, the FWHM of both GDR and PDR show increasing behavior with A , except for smaller A for GDR.

Finally, the fraction of the EWSR $m_1\%$ is also extracted. Figure 12 shows the calculated results which clearly illustrate that with the increases of mass number A or neutron-skin thickness, PDR component increases almost linearly. Similar phenomenon has been also reported earlier for some isotopes with random phase ap-

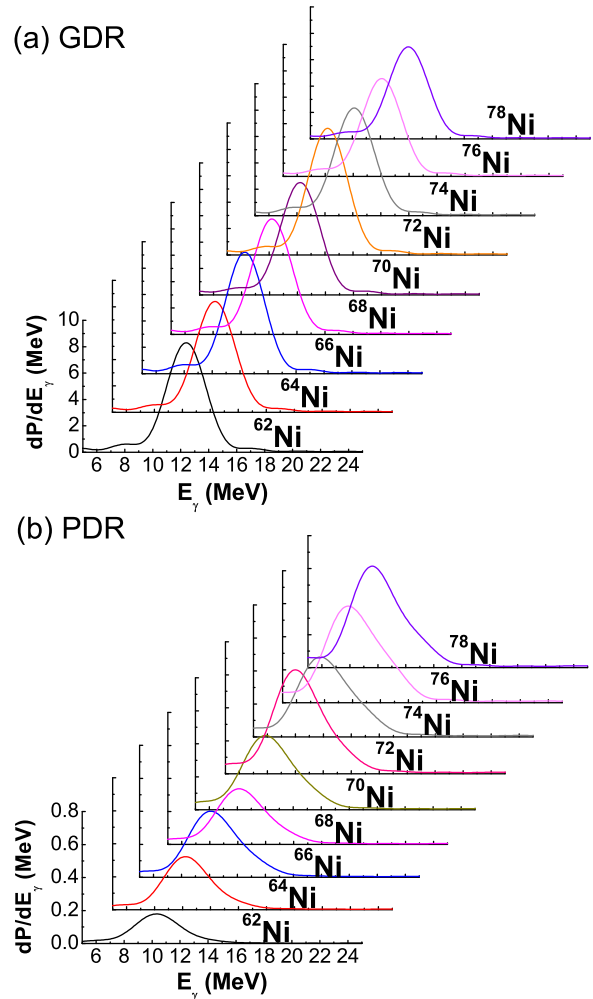


FIG. 10: (Color online) Mass number dependence of GDR (a) and PDR spectra (b) for Ni isotopes. In calculations, we use $E_{in} = 100$ MeV/nucleon, $b = 24$ fm, $C_{sym} = 32$ MeV, and the Soft EOS without MDI.

proximation phenomenological approach [20, 31, 34, 35].

IV. SUMMARY

In summary, we have applied the IQMD model to study Giant and Pygmy Dipole Resonance in Ni isotopes by the Coulomb excitation. Similar to the method to calculate Giant Dipole Resonance in our previous IQMD calculation, we extend it to calculate PDR in the same model. We first showed very stable initial projectile and target can be obtained with the soft momentum-dependent EOS, which assures the performance of GDR and RDR calculations. After we got a satisfied calculated PDR result for ^{68}Ni which agrees with the experimental data very well, then we performed a systematic calculation for GDR and PDR with different beam energy, EOS and symmetry energy parameters for $^{68}\text{Ni} + ^{197}\text{Au}$ situa-

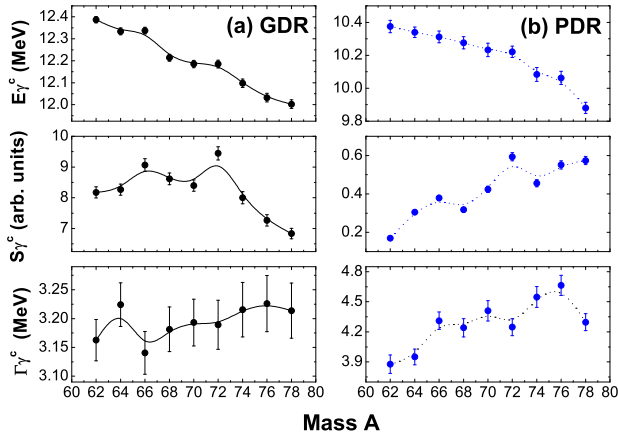


FIG. 11: (Color online) Mass number dependence of Ni isotopes of GDR (left panels) and PDR (right panels) parameters. In calculations, we use $E_{in} = 100$ MeV/nucleon, $b = 24$ fm, $C_{sym} = 32$ MeV, and the Soft EOS without MDI.

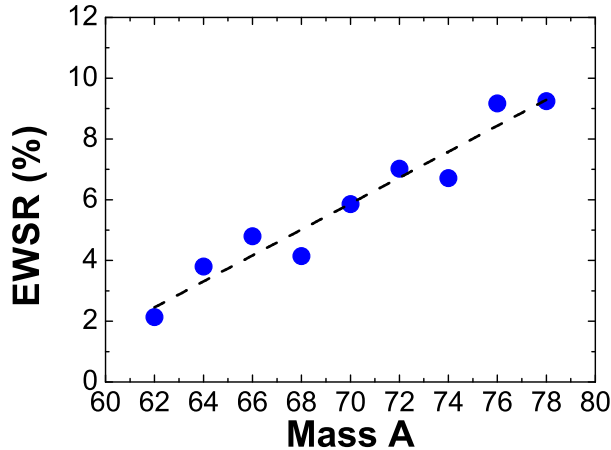


FIG. 12: (Color online) Calculated EWSR $PDR_{m1}/GDR_{m1}\%$ for Ni isotopes (solid circles) together with a linear fit (line).

tion. It is found that the peak energy and strength for both GDR and PDR show a decreasing trend with the incident energy, which can be understood by the excitation extent due to Coulomb field in different energies. When the equation of state becomes harder or momentum dependent interaction is taken into account, the increasing behaviors of peak energy, strength and FWHM emerge for both GDR and PDR. Concerning the symmetry term of EOS, it shows strong positive correlation with the GDR's peak energy and FWHM, but it plays a relative weak role on PDR. By fitting to other mean-field calculations of EWSR vs the slope parameter at saturation L_s and assuming 15% uncertainty of L_s , i.e. $L_s = 60 - 81$ MeV, we can obtain the range of symmetry energy coefficient $C_{sym} \approx 23.3 - 37.3$ MeV and symmetry energy at saturation is around 24.2 - 31.2 MeV and in the IQMD model, which gives a constraint for the QMD model. Finally, mass number or isospin dependence of GDR and PDR for the Ni isotopes is presented. The result shows that the peak energy of both GDR and PDR decreases with mass number, and the FWHM of them increases. For the strength, PDR shows an increasing behavior but GDR seemingly decrease with mass of isotopes. For the fraction of the EWSR in Ni isotopes, it shows a linear rise-up with the increases of mass number A or neutron excess.

Acknowledgements

This work was supported in part by the National Natural Science Foundation of China under Contract Nos. 11035009, 10979074, and 11205230, the Major State Basic Research Development Program in China under Contract No. 2013CB834405, the Chinese Academy of Science Foundation under Grant No. KJCX2-EW-N01.

-
- [1] B. Borderie and M. F. Rivet, Prog. Part. Nucl. Phys. **61**, 551 (2008).
 - [2] S. Das Gupta, A. Z. Mekjian and M. B. Tsang, Adv. Nucl. Phys. **26**, 89 (2001).
 - [3] J. B. Natowitz, K. Hagel, Y. G. Ma *et al.*, Phys. Rev. Lett. **89**, 212701 (2002).
 - [4] Y. G. Ma, Phys. Rev. Lett. **83**, 3617 (1999); Y. G. Ma *et al.*, Phys. Rev. C **71**, 054606 (2005); Y. G. Ma, W. Q. Shen, Nucl. Sci. Tech. **15**, 4 (2004).
 - [5] S. X. Li *et al.*, Nucl. Sci. Tech. **22**, 235 (2011); G. Q. Zhang *et al.*, Nucl. Sci. Tech. **23**, 61 (2012).
 - [6] S. Krewald, J. Speth, Int. J. Mod. Phys. E **18**, 7 (2009).
 - [7] N. Paar, D. Vretenar, E. Khan and G. Coló, Rep. Prog. Phys. **70**, 691 (2007) and references therein.
 - [8] A. Leistenschneider *et al.*, Phys. Rev. Lett. **86**, 5442 (2001).
 - [9] T. Hartmann *et al.*, Phys. Rev. Lett. **85**, 274 (2000).
 - [10] T. Hartmann *et al.*, Phys. Rev. Lett. **93**, 192501 (2004).
 - [11] O. Wieland *et al.*, Phys. Rev. Lett. **102**, 092502 (2009).
 - [12] P. Adrich *et al.*, Phys. Rev. Lett. **95**, 132501 (2005).
 - [13] S. C. Fultz *et al.*, Phys. Rev. **186**, 1255 (1969).
 - [14] N. Ryezayeva *et al.*, Phys. Rev. Lett. **89**, 272502 (2002).
 - [15] J. Liang *et al.*, Phys. Rev. C **75**, 054320 (2007).
 - [16] V. Tselyaev *et al.*, Phys. Rev. C **75**, 014315 (2007).

- [17] N. Paar *et al.*, Phys. Rev. Lett. **94**, 182501 (2005).
- [18] D. Vretenar *et al.*, Nucl. Phys. A **692**, 496 (2001).
- [19] C. Barbieri *et al.*, Phys. Rev. C **77**, 024304 (2008).
- [20] J. Piekarewicz, Phys. Rev. C **73**, 044325 (2006).
- [21] G. M. Liu, D. Fu, Y. G. Ma, W. Q. Shen, X. W. Cheng, Chin. J. Nucl. Phys. **15**, 234 (1993).
- [22] V. Baran, B. Frecus, M. Colonna, and M. Di Toro, Phys. Rev. C **85**, 051601(R) (2012).
- [23] J. Aichelin, Phys. Rep. **202**, 233 (1991).
- [24] Sakshi Gautam, Rajiv Chugh, Aman D. Sood, Rajeev K. Puri, Ch. Hartnack, J. Aichelin, J. Phys. G **37**, 085102 (2010).
- [25] C. Hartnack, R. K. Puri, J. Aichelin, J. Konopka, S. A. Bass, H. Stoecker and W. Greiner, Eur. Phys. J. A **1**, 151 (1998) .
- [26] C. Hartnack, Z. X. Li, L. Neise, G. Peilert, A. Rosenhauer, H. Sorge, H. Stoecker and W. Greiner *et al.*, Nucl. Phys. A **495**, 303c (1989).
- [27] Y. G. Ma *et al.*, Phys. Rev. C **73**, 014604 (2006).
- [28] Sanjeev Kumar, Suneel Kuma, R. K. Puri, Phys. Rev. C **81**, 014601 (2010); *ibid*, C **81**, 014611 (2010); S. Gautam and R. K. Puri, Phys. Rev. C **85**, 067601 (2012).
- [29] V. Baran *et al.*, Nucl. Phys. A **679**, 373 (2001).
- [30] H. L. Wu, W. D. Tian, Y. G. Ma *et al.*, Phys. Rev. C **81**, 047602 (2010).
- [31] A. Carbone *et al.*, Phys. Rev. C **81**, 041301(R) (2010).
- [32] A. Klimkiewicz *et al.*, Phys. Rev. C **76**, 051603(R) (2007).
- [33] M. B. Tsang *et al.*, Phys. Rev. Lett. **102**, 122701 (2009).
- [34] G. C3, V. De Donno, C. Maieron, M. Anguiano and A. M. Lallena, Phys. Rev. C **80**, 014308 (2009).
- [35] T. Inakura, T. Nakatsukasa, K. Yabana, Phys. Rev. C **84**, 021302(R) (2011).